Gold-containing bioactive glasses: a solid-state synthesis to produce alternative biomaterials for bone implantations

UNIVERSITÀ DEGLI STUDI DI TORINO

Gold-containing bioactive glasses: a solid-state synthesis to produce non-cytotoxic biomaterials for bone cells

Aina Valentina, Cerrato Giuseppina, Martra Gianmario,

[1] Department of Chemistry IFM, University of Torino, Via P. Giuria 7, 10125 Torino, Italy; Centre of Excellence NIS (Nanostructured Interfaces and Surfaces); INSTM (Italian National Consortium for Materials Science and Technology), UdR University of Torino.

Bergandi Loredana, Costamagna Costanzo, Ghigo Dario

[2] Department of Genetics, Biology and Biochemistry, University of Torino, Via Santena 5/bis, 10126 Torino, Italy.

Malavasi Gianluca,* Lusvardi Gigliola, Menabue Ledi.

[3] Department of Chemical and Geological Science, University of Modena and Reggio Emilia, Via Campi 183, 41125 Modena, Italy.

* to whom correspondence should be addressed:

Department of Chemical and Geological Science, University of Modena and Reggio Emilia, Via Campi 183, 41125 Modena, Italy, E-mail address: gmalavasi@unimo.it

Tel +390592055041; Fax +39059373543

Abstract

A new melted AuNPs-containing bioactive system was prepared exploiting a post-synthesis thermal treatment that allows to modify crystal phases and nature, shape and distribution of the gold species in the glass-ceramic matrix as evidenced by Uv-Vis, TEM and PXRD analysis. The biological tests (LDH leakage and MDA production) performed with osteoblast cells reveal that the presence of Au^{n+} species causes cytotoxicity, whereas the system HAu-600-17 containing only AuNPs does not cause any toxic effect. In addition, HAu-600-17 system showed in vitro bioactive response in terms of hydroxyapatite formation and an increase of specific surface area with a controlled release of gold species; this material is suitable to be used as model system for the controlled delivery of nanoparticles.

Keywords: gold-containing bioactive glasses; solid state synthesis; physico-chemical characterization; human MG-63 osteoblasts; cytotoxicity

Abbreviations

Nanoparticles (NPs), gold-containing NPs (AuNPs), Hench's Bioglass® 45S5 (H), gold-containing Hench's Bioglass® 45S5 (HAu), thermal treatment at 600°C for 1 h (H-600-1, HAu-600-1) and for 17 h (H-600-17, HAu-600-17), transmission electron microscopy (TEM), specific surface area (SSA), powder-X-Ray diffraction (PXRD), solid state synthesis (SSS), Brunauer Emmett and Teller (BET), inductively coupled plasma (ICP), environmental scanning electron microscopy (ESEM), energy dispersive spectrometer (EDS), lactate dehydrogenase (LDH), malonyldialdehyde (MDA)

1. Introduction

In the field of implantable biomaterials for bone and dental applications, Hench's Bioglass® 45S5 technology has undergone intensive development since 1970, when it was first proposed by Hench [1]. The production of bioactive glasses with new compositions and/or containing metallic nanoparticles (NPs) opens the door to new opportunities for medical treatments [2-3]. It is well known that the properties of NPs strongly depend on many factors, such as particle size, shape, and nature of the protecting and/or stabilizing agent [4].

The use of gold-containing NPs (AuNPs) is of great interest for many biomedical applications, such as drug delivery, imaging, and diagnostics [5-7], due to the promising properties of AuNPs, such as biocompatibility, easy synthesis, facile surface modification [8], stability and optical properties [9].

To develop successful practical applications for nano-biotechnology, a better understanding of the cytotoxic effects of AuNPs is a prerequisite. The cytotoxicity of AuNPs still remains to be clearly elucidated, being variously described in different in vitro and in vivo systems.

For instance, in vivo administered 20 nm AuNPs caused generation of oxidative stress, inflammation and DNA damage/cell death in rat brain [10], and intraperitoneally administered 10-50 nm AuNPs exerted size- and time-dependent toxic effects on rat cardiac muscle [11]. On the other hand, in ex vivo experiments where human blood cells were exposed to 30 nm anionic and cationic AuNPs the generation of reactive oxygen species was not significant [12], and in in vitro experiments where human endothelial cells were exposed to 18-65 nm AuNPs no toxic effect was observed, even at high (250 μg/ml) concentrations [13].

Furthermore, AuNPs caused genomic instability and DNA repair in human fibroblasts [14], but did not induce genotoxic effects in different rat cell types [15].

These are only some recent examples of the polymorph, variable spectrum of evidences concerning the toxicity of AuNPs, that is a function of size, concentration, surface modification, or surface charge [16], as well as of the experimental model used (for a very recent review see Pan Y. et al. [17].

Bioactive glasses containing AuNPs have been developed and they could be used both for bone tissue reconstruction due to their ability to form an apatite layer [18] and for cancer treatment due to their use in photothermal therapy or their functionalization with therapeutic and targeted peptides [19]: indeed gold can bind strongly to thiols and amines through a simple mixing process [20-21].

This research is aimed at developing new melted AuNPs-containing bioactive material exploiting a post-synthesis thermal treatment that allows to modify nature, shape and distribution of the gold species in the glass matrix. In this way it could be possible to modulate, on one hand, the size and the distribution of AuNPs (and eventually the presence of different oxidation states of gold species) on bioglass surface and, on the other hand, the formation of apatite nano-crystalline phase on the glass surface in order to obtain a promising biomaterial, in which the bioactivity of the glass is jointed to the possibility to release AuNPs. Parallel to this, the advantages of the addition of AuNPs could allow the future functionalization of bioglass with specific biomolecules and the improvement of the antimicrobial activity of AuNPs. We have also investigated if the post-synthesis thermal treatments could cause any cytotoxic effects when the bioglass interacts with the osteoblast cells in order to understand the impact of such material on cellular functions and to study the potential biocompatibility effects.

Experimental section

2.1 Glass Synthesis

Two glass systems, based on the molar composition of Hench's H-glass with molar formula $46.2SiO_2 \cdot 24.3Na_2O \cdot 26.9CaO \cdot 2.6P_2O_5$ x Au_2O (with x=0 and 0.050; the gold amount is conventionally indicated in the form Au_2O; about the real Au oxidation state see the next sections), were synthesized using the melt quenching method and are referred to in the following as Hench's Bioglass® 45S5 (H) and H Au (HAu), respectively. About 100 g of batch was obtained by mixing reagent grade Na_2CO_3, $CaCO_3$, SiO_2, $Na_3PO_4 \cdot 12H_2O$ and $HAuCl_3 \cdot 3H_2O$ in a sealed polyethylene bottle for 1 h. Premixed batch was put into a 50 mL platinum crucible and melted in an electric oven at 1350°C with a heating rate of 20°C/min. The temperature of 1350°C was kept for 1 h. The melts were cooled by pouring them into stainless steel plates. This cooling procedure consists of no-constant cooling rate and around 5 minutes are necessary for the melts to reach room temperature. Fast cooling form cracks in the glass which causes formation of glass pieces having 2×2×1 cm dimension. The glass pieces when reached room temperature were milled in agate mill jars and sieved through screens to obtain particles size in 250-500 μm range. In order to promote the thermal reduction of gold ions followed by the formation of gold nanoparticles (AuNPs) the glass powders were thermally treated at 600°C for 1 h (HAu-600-1) and 17 h (HAu-600-17). For comparison purpose the thermal treatments at 600°C for 1 h (H-600-1) and 17 h (H-600-17) were also performed on the H glass powders. The temperature of 600°C was chosen because it falls in the range between the glass transition temperature (T_g=521°C) and crystallization temperature (T_C=707°C) [22]: in this way the mobility of glass constituents should be favoured with a following thermal reduction of Au ions and nano-aggregation avoiding a complete material crystallization.

HAu powders were transparent and colourless while after thermal treatments at 600°C (both 1 h and 17 h) turn to light pink-red suggesting the Au nano-aggregation with a formation of AuNPs.

2.2 Experimental Characterization

Morphological and textural features of the powders obtained before and after the mentioned treatments were characterized by Transmission Electron Microscopy (TEM) and specific surface area (SSA) and porosity measurements. The physico-chemical characterization was performed by powder-X-Ray diffraction (PXRD) and UV-Vis spectroscopy in order to check the evolution of crystal phase after thermal treatment and to evaluate the gold ions reduction during the nano-aggregation process [2].

2.2.1 Transmission Electron Microscopy (TEM)

TEM images were obtained with a Jeol JEM 2010 equipped (operating at 200 kV, LaB6 filament). The microscope was equipped with an Oxford INCA 100 X-ray energy dispersive spectrometer (X-EDS). Samples were "dry" dispersed on lacey carbon Cu grids (200 mesh) [2].

2.2.2 Specific surface area (SSA) and porosity measurements

SSA and porosity were evaluated using a Micromeritics ASAP 2020 porosimeter (Micromeritics, Italy), by adsorption of an inert gas [krypton (Kr), for low SSA] or (N_2) at 77 K. Kr was used as the adsorptive gas for the materials prepared by solid state synthesis (SSS), which had very low surface area. Kr can be used to measure small adsorptions (and thus small surface areas) because it has a low saturation vapour pressure, and so the "dead space" correction for unadsorbed gas is also small, allowing reasonable precision in the measurement [23].

Before measurements, all samples were activated *in vacuo* (residual pressure < 10^{-3} Torr) at room temperature for 12 h in order to remove all physisorbed atmospheric contaminants. For SSA determination, data were analysed with the Brunauer, Emmett and Teller (BET) model. The accuracy of the BET method for SSA determination is known to be relatively low (even at its most accurate use, there is still a ± 5% divergence from the actual area). Instrumental accuracy and reproducibility of data obtained with modern automatic gas-volumetric instrumentation are, however, quite high [23-24].

2.2.3 Powder X-ray diffraction (P XRD)

Powder samples were analyzed, in the (2θ) range 10-50° with a PANalytical X'Pert Pro Bragg-Brentano diffractometer, using Ni-filtered Cu Kα radiation (λ) 1.5418 Å with X' Celerator detector with a time step of 50 s and a step size of 0.03˚ [2].

2.2.4 UV-Vis spectroscopy

UV-Vis spectra were obtained, in the 190–850 nm spectral range, with a UV-VIS-NIR Jasco V-570 spectrophotometer, by using the diffuse reflectance technique and a $BaSO_4$ plate as reflectance standard [2].

2.3 Sample reactivity in cellular culture medium (MEM)

To evaluate the changes of the samples after immersion in the cellular culture medium (Minimal Essential Medium Eagle with Earl's salts, MEM), samples were soaked in the amount of 250 mg of glass powders in 50 mL of MEM under magnetic stirring at 37°C as proposed by Kokubo *et al*. [25] in order to maintain homogeneous the composition of the system during the tests.

The ion concentrations in MEM are (ppm): Na^+ = 3263, K^+ = 196, Ca^{2+} = 100, Mg^{2+} = 37, Cl^- = 5239, HCO_3^- = 256, HPO_4^{2-} = 96 (31 expressed as P).

The samples after 0, 1, 4, 14 and 30 days of soaking were filtered with a Wathman membrane filter, pore size 0.45 μm, diameter = 50 mm and the solutions, after addition of 5ml of concentrate HNO_3/HCl (volume ratio 1:3) mixture, were tested by Inductively Coupled Plasma, Perkin Elmer Optima 4200 DV, USA (ICP) for determining Na, Ca, Au, Si and P contents at every time mentioned above. The filtered powders, after over-night drying at 60°C, were characterized by means of Fourier transform infrared spectroscopy (FT-IR), SSA and porosity measurements, and Environmental Scanning Electron Microscopy (ESEM) equipped with Energy Dispersive

Spectrometer (EDS) were performed in order to monitor the formation of hydroxyapatite bioactive phase on the glass surface.

2.3.2 Fourier transform infrared spectroscopy (FT-IR)

Infrared spectra were obtained using a FT-IR spectrometer (Bruker IFS 28, equipped with both MCT and DTGS detectors) in the 4000-400 cm^{-1} spectral range. The powdered materials were diluted with spectroscopic grade KBr powder (approximately 1 mg of sample to 50 mg of KBr) and pressed into pellets, to allow the observation of even the most intense bulk absorption bands. These pellets were placed in a gold envelope in a special quartz cell with KBr windows, which are transparent to infrared radiation. Transmission spectra were recorded using the DTGS detector, so that the low frequency region might be inspected. For each measurement, 128 scans at 4 cm^{-1} resolution were performed. [2]

2.3.3 Environmental Scanning Electron Microscopy (ESEM) and Energy Dispersive Spectrometer (EDS) analysis

The surface morphology of the specimens was observed by means of ESEM (FEI Quanta 200, Fei Company, The Netherlands). Images were acquired with an electrostatic voltage of 25 kV and a working distance of 9-10 mm. Microanalysis, obtained with an EDS (INCA 350, Oxford Instruments, UK) coupled to the ESEM, was also performed to identify and label the elements on the surface. EDS measurements were performed in quadruplicate of each examined particle and area of the surface; the results are presented as means (σ= 0.5%). All specimens were analysed before and after soaking in SBF for 0, 1, 4, 14 and 30 days [2].

2.4 Cellular tests

2.41. Cells and reagents

MG-63 human osteoblast cells (provided by Istituto Zooprofilattico Sperimentale "B. Ubertini", Brescia, Italy) were cultured up to confluence in 35-150 mm diameter Petri dishes with MEM supplemented with 2% foetal bovine serum (FBS), penicillin, streptomycin and L-glutamine in a humidified atmosphere containing 5% CO_2 at 37°C. H and HAu samples, obtained by thermal treatments post-synthesis, were soaked under continuous stirring in MEM for 1, 4, 14 and 30 days. Before the assays, all the samples were filtered with a Wathman membrane filter, pore size 0.45 μm and the confluent cells were incubated at the concentration of 50 μg/ml corresponding to 10 μg/cm^2 of cell monolayer for 24 h in the absence or presence of the H/HAu samples, differently treated. In our experiments, all powders were suspended in MEM, sonicated (Labsonic sonicator, 100 w, 10 s) before each incubation, and then incubated with the cells, by diluting the suspension in the dishes with complete MEM, i.e. containing also FBS and antibiotics, to different concentrations, which are indicated hereafter. This procedure does not modify the physicochemical characteristics of the samples, but ensures their better suspension in the culture medium.

The protein content of cell monolayers and cell lysates was assessed with the BCA kit from Pierce (Rockford, IL). Plasticware was from Falcon (Becton Dickinson, Franklin Lakes, NJ). Unless otherwise specified, other reagents were purchased from Sigma Aldrich (Milan, Italy).

2.4.2 Lactate dehydrogenase (LDH) leakage

To check the cytotoxic effect of the different experimental conditions described in the Results and Discussion section, LDH activity was measured on aliquots of culture supernatant and in the cell lysate at the end of the 24 h incubation time either in the absence or in the presence of the H and HAu samples, after 0, 1, 4, 14 and 30 days of glasses soaking in MEM, as also previously described. [26] Both intracellular and extracellular enzyme activities, measured spectrophotometrically as absorbance variation at 340 nm (37°C), were expressed as μmol of reduced nicotinamide adenine dinucleotide (NADH) oxidized/min/dish, then extracellular LDH activity was calculated as a percentage of the total (intracellular + extracellular) LDH activity in the dish.

2.4.3 Measurement of malonyldialdehyde (MDA)

After a 24 h incubation with bioactive glasses soaked after 0, 1, 4, 14 and 30 days in MEM, cells were washed with PBS, detached with trypsin/EDTA, and resuspended in 1 ml of PBS. The lipid peroxidation was detected by measuring the intracellular level of MDA, the end product derived from the breakdown of polyunsaturated fatty acids and related esters, with the lipid peroxidation assay kit (Oxford Biomedical Research, Oxford, MI), which uses the reaction of N-methyl-2-phenylindole with MDA in the presence of hydrochloric acid to yield a stable chromophore with maximal absorbance at 586 nm. Intracellular MDA, spectrophotometrically detected with a Packard EL340 microplate reader (Bio-Tek Instruments,USA), was expressed as pmol/mg cellular proteins [27].

2.4.4 Statistical analysis

All data in text and figures are provided as means ± SE. The results were analyzed by one-way analysis of variance and Tukey's test. $P < 0.05$ was considered significant.

3. Results and Discussion

The prepared samples, before and after thermal treatments, were thoroughly characterized with different physico-chemical techniques (TEM microscopy, SSA and porosity measurements, UV-Vis spectroscopy and PXRD). The bioactivity of the synthesized materials after different times (0, 1, 4, 14 and 30 days) in MEM has been monitored by SEM microscopy, FT-IR spectroscopy, and SSA measurements; the ions release in MEM solution has been checked through ICP analysis.

H and HAu were obtained as transparent homogeneous glasses. After the milling procedure, the obtained powders (in the range 250-500 μm) were first analyzed by ICP, in order to verify their composition, because during the melting process P-compounds could be partly volatilized. The obtained data obtained (**Table 1**) were in the range ± 0.5% with respect to the theoretical values. Moreover, a batch with a higher amount of $HAuCl_3 \cdot 3H_2O$ was prepared in order to obtain a theoretical molar concentration of Au_2O=0.2 %: however, ICP analysis, performed on this latter sample (data not reported for sake of brevity), indicated an Au_2O molar concentration near to 0.05 %. In fact, it was possible to observe the formation of yellow gold spots on the internal surface of the crucible, suggesting that *(i)* the 0.05% was the solubility limit of gold in this type of glass and *(ii)* excess gold, after reduction, forms an alloy with the platinum of the crucible.

For these reasons, (HR)TEM analysis was mainly focused on the gold nanoparticles (AuNPs) inserted in the glass structure. In **Figure 1** the images relative to HAu sample before and after thermal treatments at 600°C are reported. Only after 1 h at 600°C it was possible to observe the presence of very small Au particles (5 nm) non homogeneously dispersed in the glass matrix; in fact, AuNPs were found approximately near to the surface of the materials. After 17 h, both number and size (10 nm) of the nanoparticles slightly increased, probably due to either a growing process and/or to a coalescence of the very small particles. This behaviour had already been detected previously [2] in the case of AuNPs-containing sol-gel glasses. In the present paper, for the AuNPs melted glasses the concentration of AuNPs is lower with respect to sol-gel glasses due gold solubility limit.

SSA data (**Table 2**), carried out on all samples before MEM soaking, indicate that the post-synthesis thermal treatments halve the SSA of plain and Au-containing glasses.

PXRD analysis (**Figure 2**) performed on the samples both before and after the thermal treatments, are characteristic of an amorphous solid (before) and of a crystalline material (after) the thermal treatments. In particular, after the thermal treatment (1-17 h) the same crystalline phases ($Na_2CaSi_2O_6$ and β-$NaCaPO_4$). [22] were detected. In HAu samples after the thermal treatments the peaks ascribable to gold species could not be singled out and this is probably due to the low gold concentration.

The formation of AuNPs was further confirmed by the formation of plasmonic resonance peak characteristic of AuNPs at 530 nm [28]. In **Figure 3** the UV-Vis spectra of HAu samples before and after the thermal treatments are reported. The spectrum of HAu (before thermal treatment) is dominated by bands located around ~260 and ~310 nm, whereas the spectra of HAu samples after thermal treatments exhibit bands at around ~260, ~380 and ~530 nm. In order to assign these electronic adsorption bands to the various gold species (Au^+-oxidized form, Au^0-reduced form and Au nanoparticles), we referred to the literature concerning Au- and Ag-NPs dispersed in a glass matrix [18]. The presence of AuNPs can be correlated with the absorption band at ~530 nm, whereas Au^+ species and metallic Au (in the form of isolated atoms) give rise to bands between ~300 and ~330 nm and in the 350-430 nm spectral ranges, respectively. [18]

The UV-Vis spectrum of the HAu sample is also characterized by the presence of a weak band at ~310 nm, ascribable to Au oxidized in agreement with our previous paper [2], in which Au-containing glasses, before the thermal treatment, were characterized by the presence of both Au^{3+} and Au^+ species. After thermal treatment, the spectra of HAu-600-1 and HAu-600-17 samples exhibit specific absorptions that could be ascribed to metallic Au isolated atoms (380 nm) and AuNPs (530 nm). These spectra put into evidence the fundamental role of the thermal treatment at 600°C in order to obtain both Au reduction and the formation of metallic AuNPs. However, in the case of HAu-600-1 sample it is possible to observe a shoulder at ~310-320 nm attributed to a non-

complete reduction of Au^{+} to Au^{0}. Finally, the band located at 260 nm is assigned to the silica matrix [2].

The physico-chemical characterization study reveals that, among the various Au-containing samples, the sample with the best features to be used as implantable biomaterial could be the HAu-600-17, as this sample possesses no Au^{n+} species, but only AuNPs, which can be easily functionalized with molecules of biological interest.

For this reason, the sample HAu-600-17 and the corresponding sample without gold (H600-17) were soaked in MEM for different times (1, 4, 14 and 30 days) in order to evaluate their bioactivity.

In **Figure 4** SEM images (and the corresponding EDS spectra) of HAu-600-17 as-such and after 14 and 30 days of SBF soaking are reported. The formation of a new phase on the glass surface of H-600-17 becomes already evident after 14 days of soaking (see **Figure 4, section B**).

The corresponding SEM micrographs will not be reported: as H and HAu-600-17 samples at 0, 1 and 4 reaction times do not present significant features, in fact, in the case of H glass, after SBF reaction, the surface modifications are very similar to those detected for the HAu sample. Furthermore, the new phase formation process on HAu-600-17 sample after 14 days of reaction gives rise to the development of different superimposed layers: the internal one is mainly constituted by Si and O atoms, whereas new particles, whose morphology and composition is characteristic of hydroxyapatite (Ca/P=1.54), are observed on the most external layer.

After 30 days of MEM soaking (see **Figure 4, section C),** the glass surface is completely covered by these particles in the form of a homogeneous layer. The HAu glass surface and the Ca/P ratio became very similar to those found in the stoichiometric hydroxyapatite (Ca/P=1.64) *vs.* (Ca/P=1.67). The EDS analysis did not detect the presence of Au in any samples, and this is likely to be due to the low amount of Au in the glasses.

Figure 5 reports KBr pellet spectra obtained for both H and HAu samples before and after the thermal treatments. By the inspection of the spectra, carried out on the two glasses before the post-synthesis thermal treatment, it is possible to put into evidence the following bands: *i)* ~1450 cm^{-1}

assigned to the C–O stretching modes of carbonate species; *ii)* ~1035 cm^{-1} due to Si–O–Si stretching mode; *iii)* ~927 cm^{-1} typical of Si–O–NBO (non-bridging oxygen) stretching mode; *iv)* ~*738* cm^{-1} ascribable to C–O bending vibrations of carbonate species; *v)* ~*505* cm^{-1} typical of rocking Si–O–Si vibration.

After the post-synthesis thermal treatment at 600°C for 1 and 17 hours, a series of new spectral features appear. A sharp peak at ~1106 cm^{-1} is evident, and on the basis of its spectral behaviour and literature data [29] it might be ascribed to the asymmetric stretching vibration of PO_4^{3-} crystalline phase; moreover, the sharp peaks located at ~615, ~525 and ~446 cm^{-1} are typical of crystalline PO_4^{3-} bending modes [29-30]. These spectral features suggest that the post-synthesis thermal treatment induce the formation of nano-crystalline apatite dispersed in the glass matrix, in addition to the formation of AuNPs, as previously indicated by UV-Vis data.

Figure 6 reports KBr pellet spectra, obtained for H-600-17 and HAu-600-17 samples (**Section A** and **Section B**, respectively), before and after reaction at the different times of reaction in MEM.

Starting from the spectral patterns of the H-600-17 glass (**Figure 6, Section A**), it can be noted that, within 14 days of reaction, three main effects become quite evident: *(i)* the disappearance of the peak centred at about ~1106 cm^{-1}, characteristic of asymmetric stretching vibration of PO_4^{3-} crystalline phase; *(ii)* the disappearance of the peak centred at about ~927 cm^{-1} due to the so-called non-bridging oxygen species (NBO); *(iii)* the decrease of the peaks centred at about ~616 and ~525 cm^{-1}. These effects can be due to the partial dissolution of the glass crystalline phase, formed during the post-synthesis thermal treatment. Parallel to this, after 14 and 30 days reaction times, a resolved doublet at about ~610 and ~560 cm^{-1} appears, ascribable to the asymmetric bending phosphate modes [29] and this has been since long time recognized as symptomatic of the formation of a crystalline hydroxyapatite-like phase and thus of potential bioactivity [31].

The presence of apatite nano-crystallites is desirable in a biomaterial, because the small crystallite can ensure a better protein adsorption, as reported for vitronectin, and a nanostructured apatite phase is supporting the sample bioactivity [32-33].

These spectral features indicate that the formation of nano-crystalline apatite grown during the post-synthesis thermal treatment (necessary for the AuNPs formation) does not inhibit the glasses bioactivity, but only decreases the rate of hydroxyapatite formation, and FT-IR spectra concerning the evolution of H glass reactivity in simulated biological fluids are reported in a previous paper [2]. This is a positive effect because, in this way, it is possible to obtain a slow and controlled release of ions and also of AuNPs.

In the case of the HAu-600-17 sample (see **Figure 6, Section B**), the same spectral features observed for H-600-17 glass at different reaction times are evident: in fact crystalline forms of Ca-phosphate of the hydroxyapatite-like type are developed on the glass surface at 14 days of reaction in MEM, as evidenced by the presence of the former IR spectral features (compare, for istance, the curves of Figure 5, section A with those of Section B).

SSA measurements were also carried out on the samples H-600-17 and HAu-600-17 after the different reaction times (**Table 2**). Concerning the H-600-17 sample, its SSA reaches the highest value (121 m^2/g) after 14 days of soaking, whereas it decreases (88 m^2/g) after 30 days. This is a clear indication that until 14 days the glass dissolution phenomenon prevails, whereas after 30 reaction days the rate of glasses dissolution decreases with the subsequent deposition and crystallization of the hydroxyapatite layer on the glass surface.

Concerning the HAu-600-17 sample, the increase of SSA is slower than for the H-600-17 glass, this is an indication of a slower ions release and slower glass reactivity as well. Also for this sample, the SSA reaches the highest value (85 m^2/g) after 14 days of soaking and then decreases (71 m^2/g).

The ICP analysis performed on MEM solutions after different soaking times is reported in **Table 3**.

The trend of the species concentrations in MEM solution after soaking shows a similar behaviour for both samples (H-600-17 and HAu-600-17) (**Table 2**). Sodium and calcium concentration increased monotonically as a function of the soaking time in all samples, whereas the phosphate concentration becomes lower and the lowest value was detected after 14 days, in good agreement with both SEM and FT-IR analysis, indicating the formation of a new phosphate-rich phase after 14

days. The slightly increase of phosphate species concentration after 30 days can be due to a partial dissolution of internal glass matrix: it is interesting to note that Au species were detected in solution in a very low concentration (near to the value of the lowest standard, 0.10 ppm) after longer time (30 days). The Au concentration in MEM after 30 days of soaking correspond around 0.1% of the total amount present in the HAu-600-17 sample. This suggests a controlled and low release of gold.

Among all synthesised samples, the HAu-600-17 is the best candidate to be functionalized with drugs and/or biomolecules in order to be used for either bone and/or dental implants, due to both its physico-chemical and biological properties. For this reason, a biological analysis was performed on all samples before MEM soaking (0 day) and only on HAu glass after thermal treatment at 600°C for 17 h (HAu-600-17) and H glass after thermal treatment at 600°C for 17 h (H-600-17), the corresponding reference sample, both after soaking samples under continuous stirring in MEM (1, 4, 14 and 30 days).

After a 24 h-incubation in the presence of H, used as reference material, H-600-1 and H-600-17 at the concentration of 50 μg/ml (corresponding to 10 μg/cm^2 of cell monolayer), MG-63 cells did not show a significant increase of LDH activity in their extracellular medium vs. the control (**Figure 7**). On the contrary, HAu and HAu-600-1 glasses induced a significant leakage of LDH in the culture medium, that is a sensitive index of cytotoxicity (**Figure 7**). This cytotoxic effect is probably due to the presence of Au^{n+} species at the glass surface, as these species would tend to reduce themselves to Au^0, causing an oxidative stress when they are in contact with the cells. In fact, the highest value of oxidative stress occurs in the HAu sample which has the highest Au^{n+} content (see UV-vis section). In the case of HAu-600-1 sample, after 1 hour of post-synthesis thermal treatment, only few residual Au^{n+} species are still present and these might be responsible of the small increase of LDH leakage. Finally, as to HAu-600-17, no significant increase of LDH is detectable compared to the control; in this sample the thermal treatment at 600°C for 17 hours reduces all the Au^{n+} residues to Au^0. This result confirms that the Au^{n+} species are responsible of the cytotoxic effects: the surface modifications (see FT-IR spectra and SEM micrographs) that occur at the glass surface

during the dissolution process and the release of low concentrations of AuNPs (see ICP data) do not cause cytotoxic effects.

The intracellular MDA values, used as an index of cell lipoperoxidation, show the same trend of LDH release (**Figure 8**), confirming that HAu glass after thermal treatment at 600°C for 17 h could be used as a performing and implantable biomaterial.

Conclusions

A new bioactive glass-ceramic containing $Na_2CaSi_2O_6$ and β-$NaCaPO_4$ crystals and metallic gold nanoparticles (sized up to 20 nm) was obtained after post-synthesis calcination of bioactive glass.

The bioactivity tests, carried out in MEM, proved the formation of HA at the sample surface and point out their ability for generation of bone matrix.

The biological tests (LDH leakage and MDA production) performed with osteoblast cells reveal that the presence of Au^{n+} species causes cytotoxicity, whereas HAu-600-17 containing only AuNPs does not cause any toxic effect.

In summary, our data demonstrate that this novel type of gold-containing bioactive material is well suited to serve as model system for the controlled delivery of nanoparticles. Our future studies are aimed at synthesizing and validating the efficacy of this non cytotoxic gold-containing bioactive glass after a conjugation process with proteins or drugs to improve its biocompatibility.

Acknoledgements

This work was financially supported by the Italian Ministry MUR (Project COFIN-2006, Prot. 2006032335_004: “Interface phenomena in silica-based nanostructured biocompatible materials contacted with biological systems”) and by Compagnia San Paolo, Italy (Project Id: ORTO11RRT5), whose contribution is gratefully acknowledged.

References

[1] Rahaman, M.N. Day, D.D., Sonny Bal, B., Fu, Q., Jung, S.B., Bonewald L.F., Tomsia, A.P. 2011 Bioactive glass in tissue engineering. Acta Biomat. 7, 2355-2373.

[2] Lusvardi, G., Malavasi, G., Aina, V., Bertinetti, L., Cerrato, G., Magnacca, G., Morterra, C., Menabue, L. 2011 Bioactive Glasses Containing Au Nanoparticles. Effect of Calcination Temperature on Structure, Morphology, and Surface Properties. Lang. 26, 10303-10314

[3] Siqueira, R.L., Peitl, O., Zanotto, E.D. 2011 Gel-derived SiO_2-CaO-Na_2O-P_2O_5 bioactive powders: Synthesis and in vitro bioactivity. Mater. Sci. Eng. C 31, 983-991.

[4] Daniel, M.C., Astruc, D. 2003 Gold nanoparticles: Assembly, supramolecular chemistry, quantum-size-related properties, and applications toward biology, catalysis, and nanotechnology. Chem. Rev. 104, 293–346.

[5] Hainfeld, J.F., Slatkin, D.N., Focella, T.M., Smilowitz, H.M. 2006 Gold nanoparticles: a new X-ray contrast agent. Br. J. Radiol., 79, 248−253.

[6] Sperling, R.A., Gil, P., Zhang, F., Zanella, M., Parak, W.J. 2008 Biological applications of gold nanoparticles. Chem. Soc. Rev. 37, 1896−1908.

[7] Lim, Z.Z.J., Li, J.E.J., Ng, C.T., Yung, L.Y.L., Bay, B.H. 2011 Gold nanoparticles in cancer therapy. Acta Pharmacol. Sin., 32, 983−990.

[8] Lee,Y., Geckeler, KE. 2012 Cytotoxicity and cellular uptake of lysozyme-stabilized gold nanoparticles. J Biomed Mater Res A. 100, 848-855.

[9] Boisselier, E., Astruc, D. 2009 Gold nanoparticles in nanomedicine: preparations, imaging, diagnostics, therapies and toxicity. Chem. Soc. Rev. 38, 1759–1782.

[10] Siddiqi, N.J., Abdelhalim, M.A., El-Ansary, A,K,, Alhomida, A.S., Ong, W.Y. 2012 Identification of potential biomarkers of gold nanoparticle toxicity in rat brains**.** J Neuroinflammation. 9, 123-139.

[11] Abdelhalim, MA. 2011 Exposure to gold nanoparticles produces cardiac tissue damage that depends on the size and duration of exposure. Lipids Health Dis. 10, 205-214.

[12] Love, SA., Thompson, JW., Haynes, CL. 2012 Development of screening assays for nanoparticle toxicity assessment in human blood: preliminary studies with charged Au nanoparticles. Nanomedicine (Lond).

[13] Freese, C., Gibson, MI., Klok, HA., Unger, RE., Kirkpatrick, CJ. 2012 Size- and coating-dependent uptake of polymer-coated gold nanoparticles in primary human dermal microvascular endothelial cells. Biomacromolecules. 13, 1533-1543.

[14] Li, JJ., Lo SL., Ng, CT., Gurung, R.L., Hartono, D., Hande, MP. 2011 Genomic instability of gold nanoparticle treated human lung fibroblast cells. Biomaterials 32, 5515–5523.

[15] Downs, TR., Crosby, ME., Hu, T., Kumar, S., Sullivan, A., Sarlo, K., Reeder, B., Lynch, M., Wagner, M., Mills, T., Pfuhler, S. 2012 Silica nanoparticles administered at the maximum tolerated dose induce genotoxic effects through an inflammatory reaction while gold nanoparticles do not. Mutat Res. 745, 38-50.

[16] Mironava, T., Hadjiargyrou, M., Simon, M., Jurukovski, V., Rafailovich, MH. 2010. Gold nanoparticles cellular toxicity and recovery: effect of size, concentration and exposure time. Nanotoxicol. 4, 120–137.

[17] Pan, Y., Bartneck, M., Jahnen-Dechent, W. 2012 Cytotoxicity of gold nanoparticles. Methods Enzymol. 509, 225-242.

[18] Simon S. Ciceo-Lucacel, R., Radu, T., Baia, L., Ponta, O., Lepure, A., Simon, V. 2012 Gold nanoparticles developed in sol-gel derived apatite-bioactive glass composites. J. Mater. Sci: Mater. Med. 23, 1193-1201.

[19] Kumar, A. Ma, H., Zhang, X., Huang, K., Jin, S., Liu, J., Wei, T., Cao, W. Zou, G., Liang X.J. 2012 Gold nanoparticles functionalized with therapeutic and targeted peptides for cancer treatment. Biomaterials, 33, 1180-1189.

[20] Daniel, M.C., Astruc, D. 2004 Gold nanoparticles: Assembly, supramolecular chemistry, quantum-size-related properties, and applications toward biology, catalysis, and nanotechnology. Chem. Rev. 104, 293–346.

[21] Dhar, S., Daniel, W.L., Giljohann, D.A., Mirkin, C.A., Lippard, S., 2009 Polyvalent Oligonucleotide Gold Nanoparticle Conjugates as Delivery Vehicles for Platinum(IV) Warheads. J. Am. Chem. Soc. 131, 14652–14653.

[22] Linati, L., Lusvardi, G., Malavasi, G., Menabue L., Menziani, M.C., Mustarelli, P., Segre, U. 2005 Qualitative and quantitative structure-property relationships analysis of multicomponent potential bioglasses. J. Phys. Chem. B 109, 4989-4998.

[23] Gregg, S.H., Sing, K.S.W. 1967 Adsorption Surface Area and Porosity, Academic Press, New York.

[24] Lusvardi G., Malavasi, G., Menabue, L., Aina, V., Morterra, C. 2009 Fluoride-containing bioactive glasses: Surface reactivity in simulated body fluids solutions. Acta Biomaterialia 5, 3548–3562.

[25] Kokubo, T., Takadama, H., 2006 How useful is SBF in predicting in vivo bone bioactivity? Biomaterials 27, 2907-2915.

[26] Aina, V., Perardi, A., Bergandi, L., Malavasi, G., Menabue, L., Morterra, C., Ghigo, D. 2007 Cytotoxicity of zinc-containing bioactive glasses in contact with human osteoblasts. Chem. Biol. Interact. 167, 207–218.

[27] Gerard-Monnier, D., Erdelmeier, I., Regnard, K., Moze-Henry, N., Yadan, J.C., Chaudiere, J. 1998 Reactions of 1-methyl-2-phenylindole with malondialdehyde and 4-hydroxyalkenals. Analytical applications to a colorimetric assay of lipid peroxidation. Chem. Res. Toxicol. 11 1176–1183.

[28] Burda, C., Chen, X., Narayanan, R., El Sayed, M.A, 2005 Chemistry and properties of nanocrystal of different shape. Chem. Rev. 105, 1025-1032.

[29] Sygnatowicz, M., Tiwari, A. 2009 Controlled synthesis of hydroxyapatite-based coatings for biomedical application. J. Mat. Sci. and Eng. C 29, 1071–1076.

[30] Kumar Singh, R., Kothiyal, G.P., Srinivasan A. 2009 In vitro evaluation of bioactivity of $CaO–SiO_2–P_2O_5–Na_2O–Fe_2O_3$ glasses Applied Surface Science 255, 6827–6831.

[31] Kothiyal, G.P., Srinivasan, A. 2009 In vitro evaluation of bioactivity of $CaO–SiO_2–P_2O_5–Na_2O–Fe_2O_3$ glasses Applied Surface Science 255, 6827–6831.

[32] Fujii, E., Ohkubo, M., Tsuru, K., Hayakawa, S., Osaka, A., Kawabata, K., Bonhomme, C., Babonneau, F. 2006 Selective protein adsorption property and characterization of nano-crystalline zinc-containing hydroxyapatite. Acta Biomater. 2, 69–74.

[33] Webster, T.J., Ergun, C., Doremus, R.H., Siegel, R.W., Bizios, R. 2000 Specific proteins mediate enhanced osteoblast adhesion on nanophase ceramics. J. Biomed. Mater. Res. 51, 475–483.

Figure Captions

Figure 1. Transmission electron microscopy (TEM) images carried out on gold-containing samples before (HAu) and after the thermal treatments at 600°C for 1 (HAu-600-1) and 17 hours (HAu-600-17).

Figure 2. PXRD spectra of the Au-containing system before (HAu) and after (HAu-600-1 and HAu-600-17) the thermal treatment.

Figure 3. UV-Vis spectra carried out on HAu samples before and after the thermal treatment at 600°C for 1 and 17 hours.

Figure 4. Scanning electron microscopy (SEM-EDS analysis) performed on H-600-17 as such (Section **A**) and HAu-600-17 samples after 14 (Section B) and 30 days in MEM solution (Section C).

Figure 5. FT-IR spectra (KBr pellet method; in the 1800-400 cm^{-1} spectral range) collected onto all prepared samples (before and after the thermal treatments and with or without gold).

Figure 6. FT-IR spectra (KBr pellet method; in the 1800-400 cm^{-1} spectral range) collected onto H-600-17 (Section A) and HAu-600-17 (Section B) glasses after different times of soaking in MEM solution.

Figure 7. Effect of various glass powders on MG-63 cells in terms of LDH release in the supernatant. Cells were incubated for 24 h in the absence (CTRL) or presence of one of the following bioactive glasses (50 μg/ml, 12.5 $\mu g/cm^2$ cell monolayer): Hench's Bioglass® 45S5 (H), H glass after thermal treatment at 600°C for 1 h (H-600-1), H glass after thermal treatment at 600°C for 17 h (H-600-17) and Hench's Bioglass® 45S5 containing Au (HAu), HAu glass after thermal treatment at 600°C for 1 h (HAu-600-1) and HAu glass after thermal treatment at 600°C for 17 h (HAu-600-17), samples that are all obtained from different times of reaction in MEM (0, 1, 4, 14, 30 days). After the incubation time the LDH activity was measured as described in Materials and Methods. Extracellular LDH activity was calculated as percentage of total (intracellular +

extracellular) LDH activity in the dish. Measurements (n = 3) were performed in triplicate, and data are presented as means ± SE. Vs. CTRL **p < 0.001; *p < 0.0001.

Figure 8. Effect of various glass powders on MG-63 cells in terms of MDA production. Cells were incubated for 24 h in the absence (CTRL) or presence of one of the following bioactive glasses (50 μg/ml, 12.5 μg/cm^2 cell monolayer): Hench's Bioglass® 45S5 (H), H glass after thermal treatment at 600°C for 1 h (H-600-1), H glass after thermal treatment at 600°C for 17 h (H-600-17) and Hench's Bioglass® 45S5 containing Au (HAu), HAu glass after thermal treatment at 600°C for 1 h (HAu-600-1) and HAu glass after thermal treatment at 600°C for 17 h (HAu-600-17), samples that are all obtained from different times of reaction in MEM (0, 1, 4, 14, 30 days). After the incubation time the MDA production was evaluated, as described in Materials and Methods. Measurements (n = 3) were performed in triplicate, and data are presented as means ± SE. Vs. CTRL **p < 0.001; *p < 0.0001.

Figures

Figure 1.

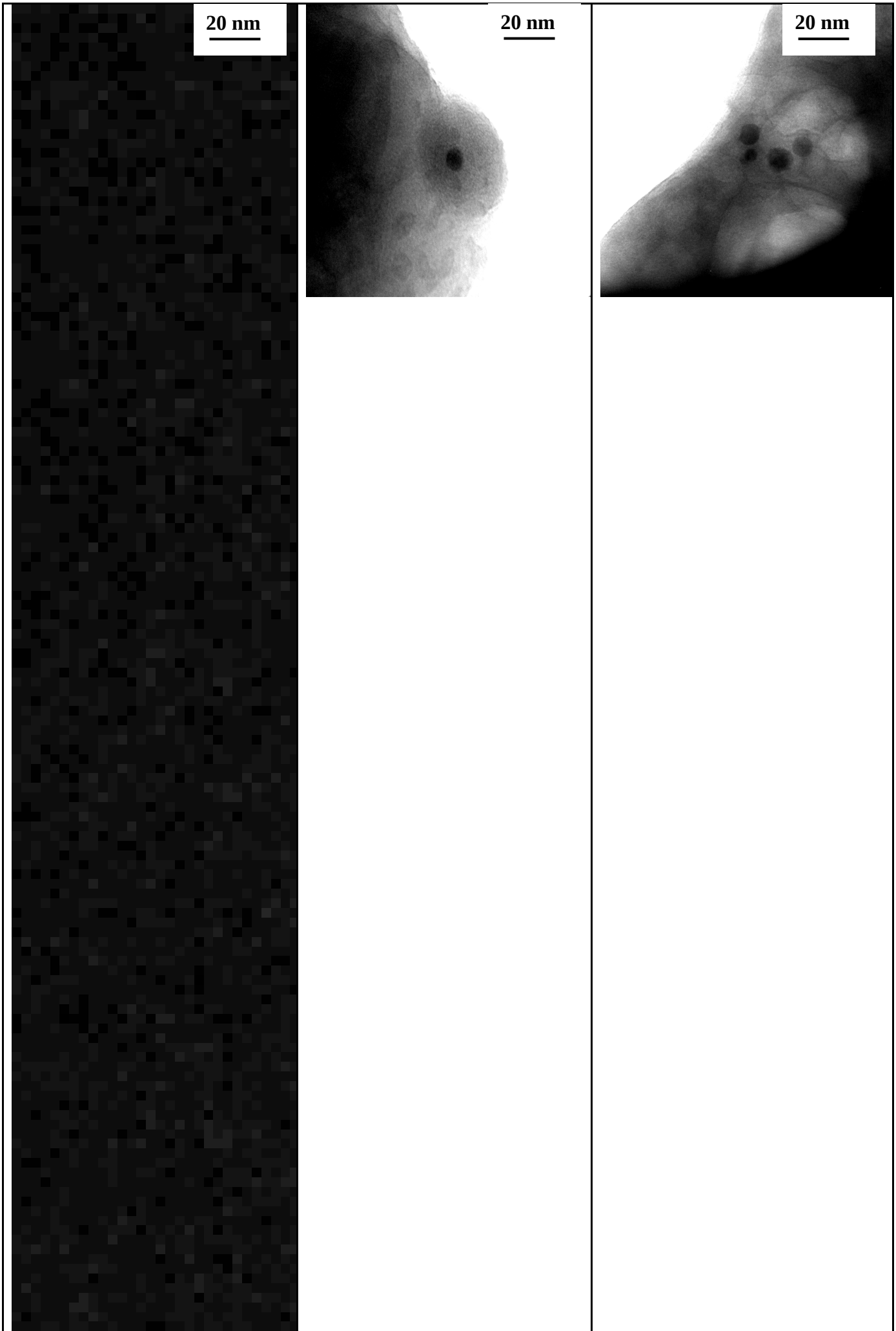
20 nm
20 nm
20 nm

a) HAu	b) HAu-600-1	c) HAu-600-17

Figure 2.

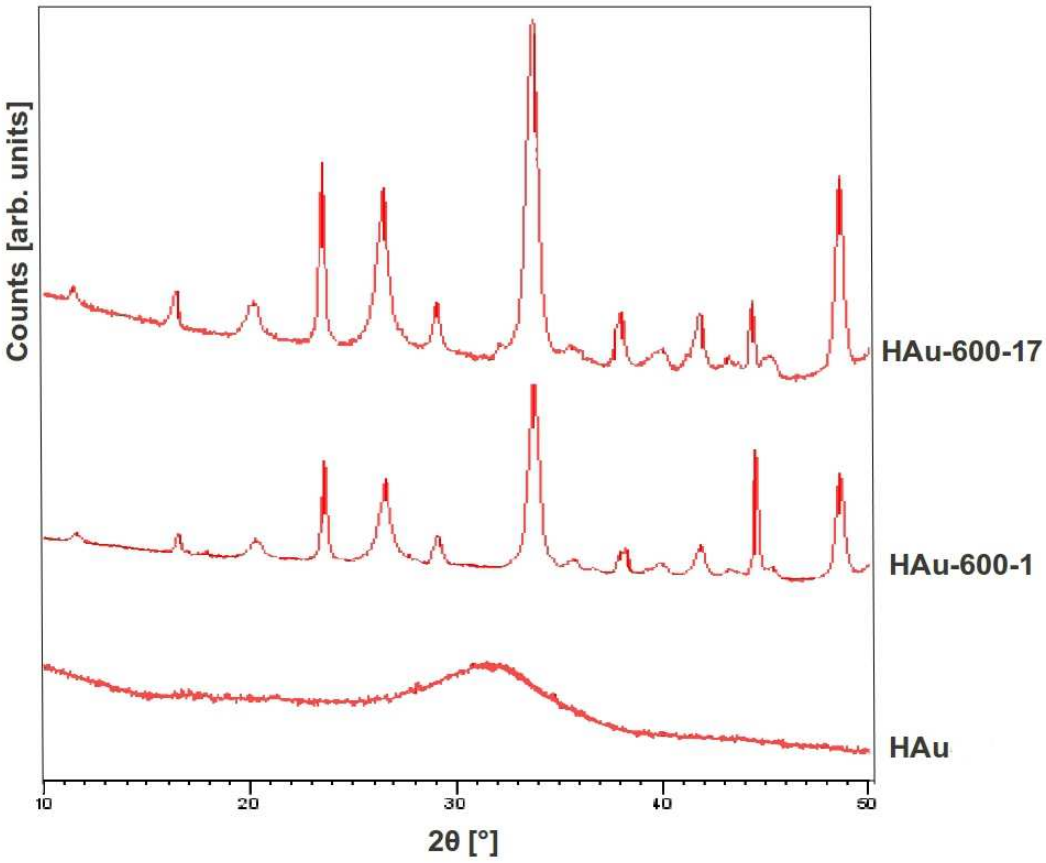
Counts [arb. units]
HAu-600-17
HAu-600-1
HAu
10
20
30
40
50
2θ [°]

Figure 3.

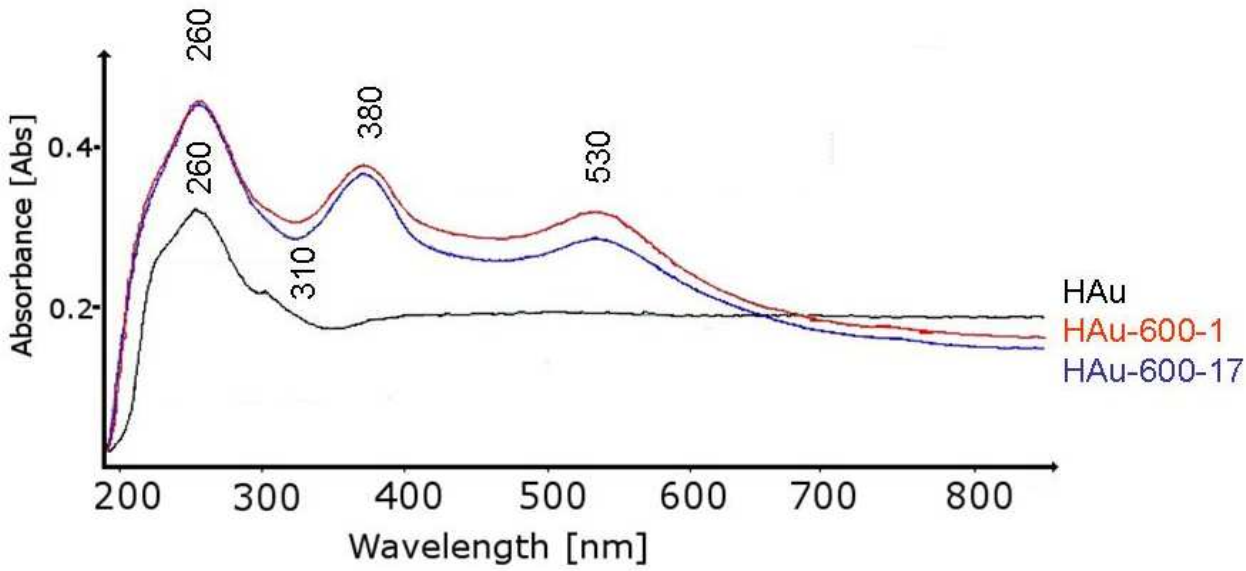
260
380
530
260
310
Absorbance [Abs]
0.4
0.2
200
300
400
500
600
700
800
Wavelength [nm]
HAu
HAu-600-1
HAu-600-17

Figure 4.

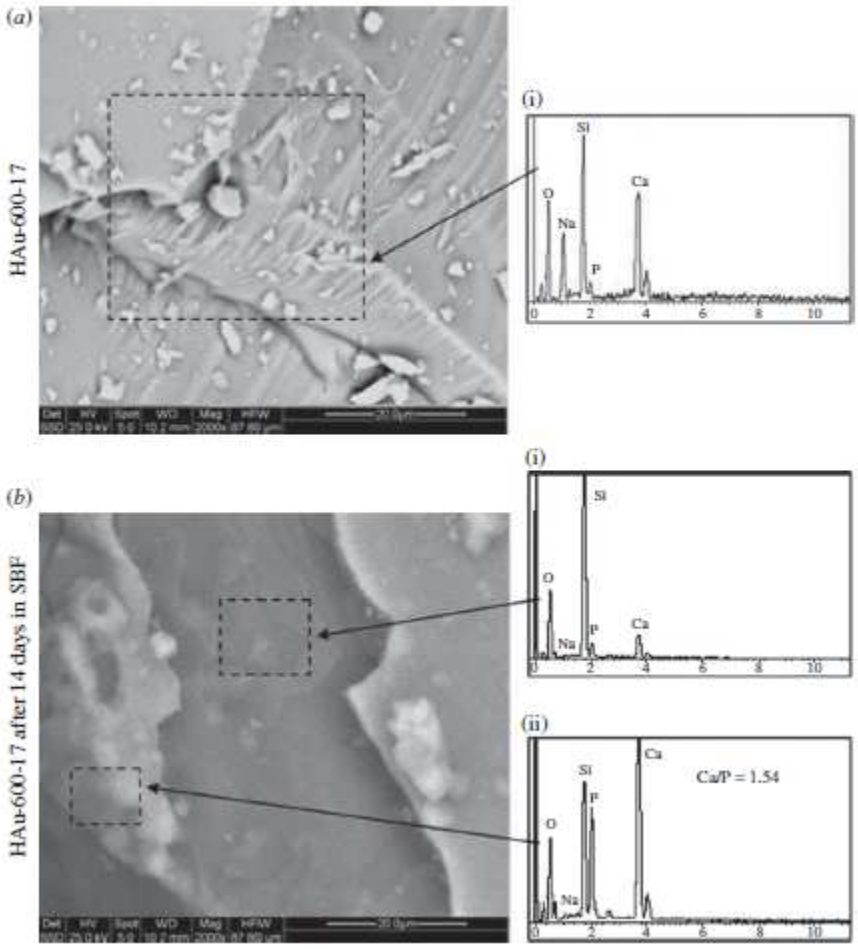
(a)
HAu-600-17
(i)
Si
O
Na
P
Ca
0
2
4
6
8
10
(b)
HAu-600-17 after 14 days in SBF
(i)
Si
O
Na
P
Ca
(ii)
Ca
Si
P
O
Na
Ca/P = 1.54

Figure 5.

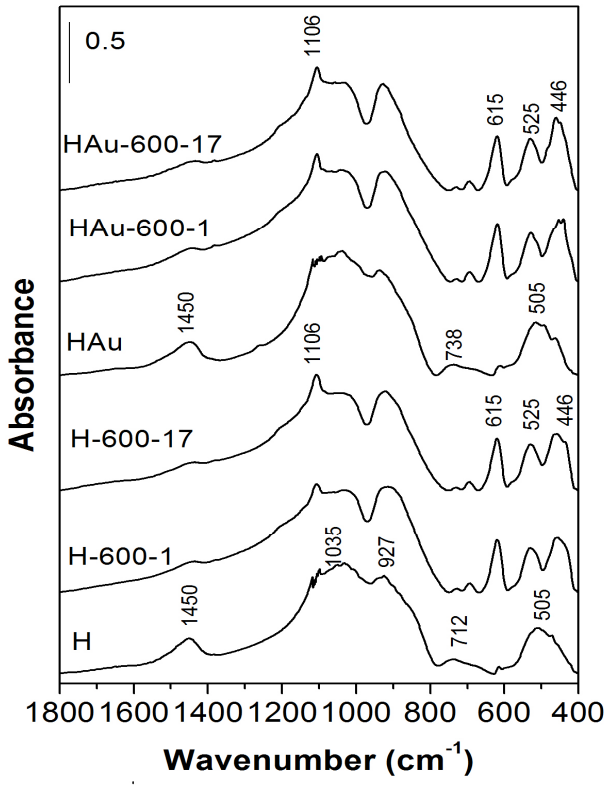
0.5
1106
615
525
446
HAu-600-17
HAu-600-1
1450
505
HAu
738
1106
615
525
446
H-600-17
H-600-1
1035
927
1450
505
712
H
Absorbance
1800 1600 1400 1200 1000 800 600 400
Wavenumber (cm-1)

Figure 6.

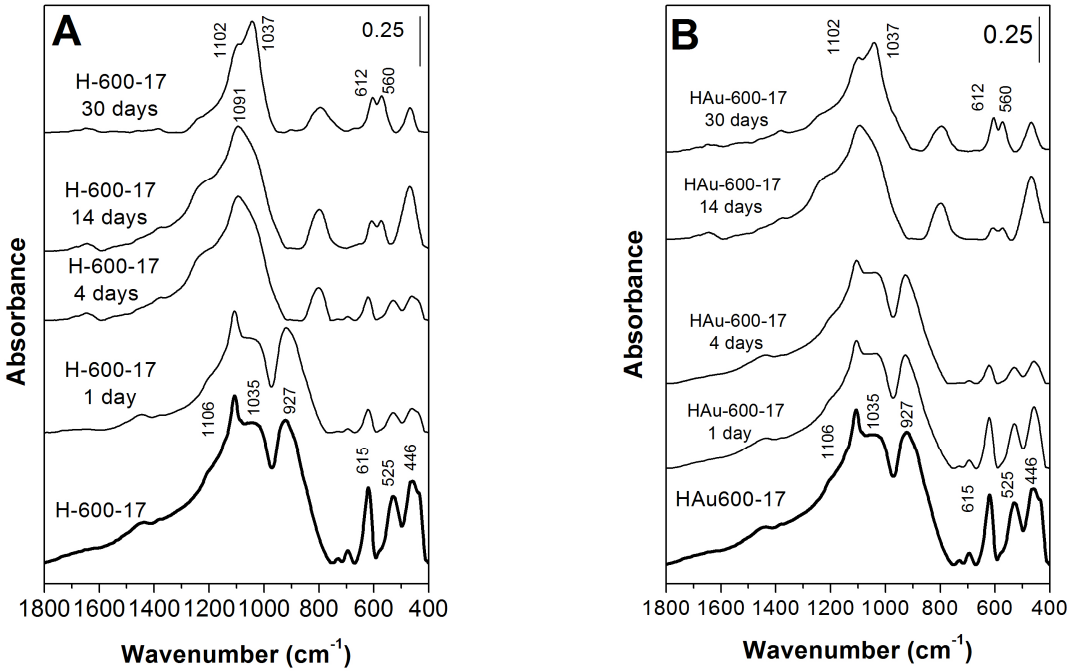
A
0.25
1102
1037
1091
612
560
H-600-17
30 days
H-600-17
14 days
H-600-17
4 days
H-600-17
1 day
1106
1035
927
615
525
446
H-600-17
Absorbance
1800 1600 1400 1200 1000 800 600 400
Wavenumber (cm-1)
B
0.25
1102
1037
612
560
HAu-600-17
30 days
HAu-600-17
14 days
HAu-600-17
4 days
HAu-600-17
1 day
1106
1035
927
615
525
446
HAu600-17
Absorbance
1800 1600 1400 1200 1000 800 600 400
Wavenumber (cm-1)

Figure 7.

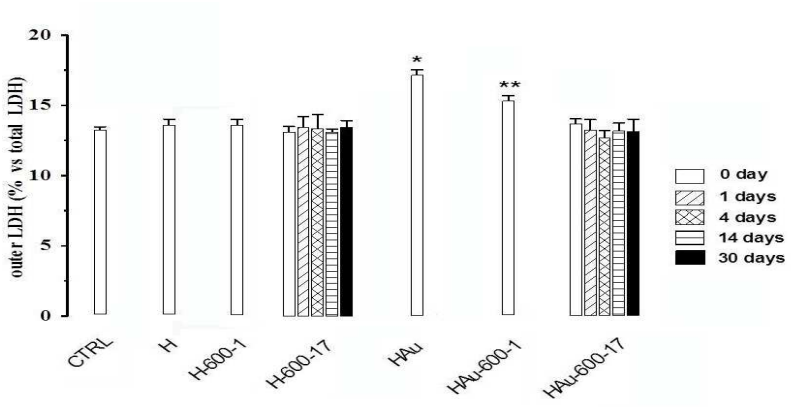
outer LDH (% vs total LDH)
20
15
10
5
0
*
**
0 day
1 days
4 days
14 days
30 days
CTRL
H
H-600-1
H-600-17
HAu
HAu-600-1
HAu-600-17

Figure 8.

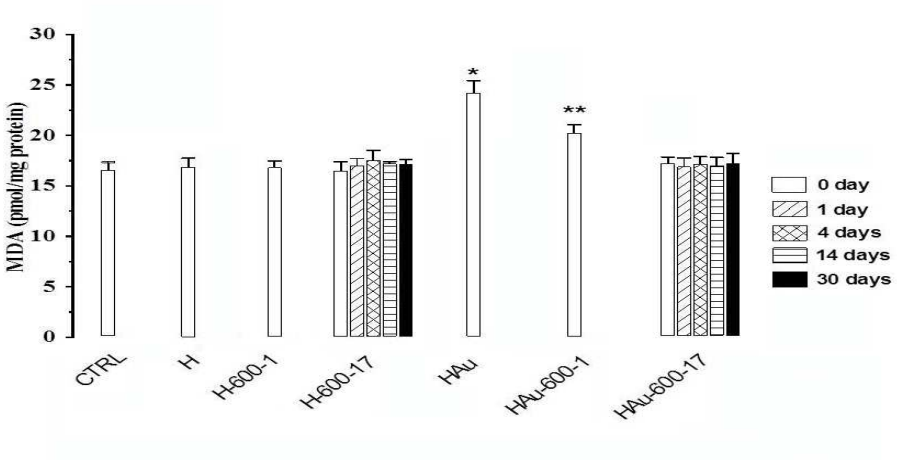
MDA (pmol/mg protein)
30
25
20
15
10
5
0
*
**
0 day
1 day
4 days
14 days
30 days
CTRL
H
H-600-1
H-600-17
HAu
HAu-600-1
HAu-600-17

Tables.

Table 1. Experimental sample compositions (as % mol) and samples description.

	Composition (% mol)					Post-synthesis treatment
	SiO_2	Na_2O	CaO	P_2O_5	Au_2O	
H samples						
H	46.2	24.3	26.9	2.6		/
H-600-1	46.7	24.1	26.7	2.5		1 hour at 600°C
H-600-17	46.7	24.1	26.7	2.5		17 hours at 600°C
HAu samples						
HAu	46.2	24.3	26.9	2.6	0.050	/
HAu-600-1	46.4	24.8	25.9	2.8	0.046	1 hour at 600°C
HAu-600-17	46.3	24.6	26.5	2.6	0.046	17 hours at 600°C

Table 2. Specific surface area **(**SSA) data of the sample as such and after reaction in MEM solution.

Samples	**BET SSA m^2/g (Kr)**	**BET SSA m^2/g (N_2)**
H samples		
H	0.76	
H-600-1	0.32	
H-600-17	0.35	
H-600-17 (1 day in MEM)	10	
H-600-17 (4 days in MEM)		50
H-600-17 (14 day in MEM)		121
H-600-17 (30 day in MEM)		88
HAu samples		
HAu	0.64	
HAu-600-1	0.39	
HAu-600-17	0.37	
HAu-600-17 (1 day in MEM)	1.30	
HAu-600-17 (4 days in MEM)		28
HAu-600-17 (1 day in MEM)		85
HAu-600-17 (1 day in MEM)		71

Table 3. ICP analysis performed in MEM solution after different soaking times (1, 4, 14 and 30 days).

Sample	Days	Si [ppm] ±5%[a]	Na [ppm] ±2%[a]	Ca [ppm] ±5%[a]	P [ppm] ±5%[a]	Au [ppm] ±3%[a]
MEM (starting concentration)		0	3220	70	30	0
H-600-17	1	64	3237	154	26	0,00[b]
	4	53	3274	187	11	0,00[b]
	14	56	3347	194	0,3	0,00[b]
	30	53	3545	226	0,7	0,00[b]
HAu-600-17	1	65	325	130	26	0,00[b]
	4	60	3315	168	12	0,00[b]
	14	58	3359	193	0,2	0,00[b]
	30	56	3541	274	0,5	0,12

[a]: standard deviation obtained by three measurements performed on the solutions.

[b]: values lower than the lowest standard (0.10 ppm).